Langmuir

Article

pubs.acs.org/Langmuir

# Gravitational Drainage of Foam Films

S. Sett, S. Sinha-Ray, and A. L. Yarin*

Department of Mechanical and Industrial Engineering, University of Illinois at Chicago, 842 West Taylor Street, Chicago, Illinois 60607-7022, United States

**ABSTRACT:** Gravitational drainage from thick plane vertical soap films and hemispherical bubbles is studied experimentally and theoretically. The experiments involve microinterferometry kindred to the one used in the experiments in the Scheludko cell. The following surfactants were used in the experiments: cationic dodecyltrimethylammonium bromide (DTAB), anionic sodium dodecyl sulfate (SDS), anionic Pantene shampoo which primarily contains sodium lauryl sulfate, nonionic tetraethylene glycol monooctyl ether ($C_8E_4$), and nonionic Pluronic (P-123) surfactants at different concentrations. The theoretical results explain the drainage mechanism and are used to develop a new method of measurement of the surface elasticity and to test it on the above-mentioned surfactants.

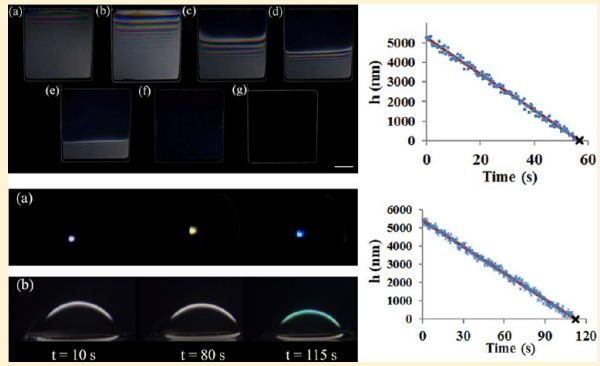


## INTRODUCTION

Liquid drainage from foam films is a complex, intriguing, and practically important phenomenon. It is associated with the interplay of viscous flow of solvent, diffusion and convection of surfactant molecules, and their adsorption and desorption at the film interfaces and the associated changes in the surface tension as well as the appearance of the concentration-dependent surface tension gradients leading to the Marangoni effect equivalent to the surface elasticity. In addition, surface viscosity of thick (e.g., protein-stabilized) interfaces can also be of importance. Moreover, when the draining films become sufficiently thin (about and below 100 nm), the disjoining pressure becomes important, and its steric, electric, and van der Waals components affect the film thinning and contribute either to its deceleration (stabilization) or localized acceleration (destabilization). Such a plethora of physical phenomena entangled with the solvent drainage driven by different fluid mechanical mechanisms (capillary pressure, gravity, wave propagation) kept foam films in focus for at least 60 years. Different physical aspects of the prior foam drainage research are covered in several monographs, collective works, and review articles,[1−13] whereas the applied aspects of foam stabilization by surfactants, proteins, and nanoparticles are exposed in a number of review articles.[14−16]

Capillary-driven drainage of horizontal circular films trapped in the Scheludko cell was one of the main tools in studying surface elasticity of foams.[7,12,17−24] The microinterferometry, assisted with CCD camera recording and digital filtering, allowed for elucidation of the capillary drainage of parallel-surface and wavy films down to the black films of thicknesses of the order of 30 nm.[17−21] Not only fully freely suspended films with two free surfaces were studied[17−21] but also capillary drainage of films with one free surface supported on a glass slide was explored.[22] These results were used to evaluate the validity ranges of the existing theories of capillary-driven film drainage including the effects of the different components of the disjoining pressure.[23,24] An important result of the capillary drainage experiments in the Scheludko cell was the elucidation of the surface elasticity characterizing the strength of the surfactant-concentration-driven Marangoni effect. The role of the dissolved air bubbles on the film rupture was also elucidated.

Gravity-driven drainage of spherical bubbles located at the free surface of a liquid pool was studied experimentally and theoretically for polymer melts where a long life of a bubble is associated with very high viscosity, rather than with the presence of surfactants in distinction from the soap film/bubbles.[25]

Surprisingly, gravity-driven drainage attracted much less attention than the capillarity-driven one. Formation of a "young" soap film withdrawn on a vertically oriented wire frame was addressed as a phenomenon in which a film is still connected to the pool and supported against gravity by the osmotic pressure, while convection driven by gravity was neglected.[26] Drainage of foam in a gravity settler is associated with gravity-driven viscous flow of water along the Plateau borders.[27] This type of foam drainage was recently revisited in the framework of the consolidation theory which includes viscous resistance to the gravity-driven flow and the overall medium elasticity associated with air in the bubbles but does not incorporate the film surface elasticity (the Marangoni effect).[28] In addition, flowing foams in porous media not only reveal a plethora of physical mechanisms responsible for foam rupture, such as coarsening due to air diffusion through the

**Received:** January 23, 2013
**Revised:** March 22, 2013
**Published:** April 4, 2013

   dx.doi.org/10.1021/la4003127 | *Langmuir* 2013, 29, 4934−4947

liquid lamella from smaller to larger bubbles, various instability mechanisms, etc.,[29] but also expose the importance of the concentration-driven Marangoni effect.[30]

The present work aims at the gravity-driven drainage of vertical films of surfactant solutions withdrawn on a frame from a pool as well as at spherical bubbles located at the pool surface, with special attention paid to the surface elasticity and its measurement. The next section describes the materials and the experimental setup, followed by a section on the theoretical aspects. This is followed by results and discussion and finally conclusions are drawn.

## EXPERIMENTAL SECTION

**Materials.** The following surfactants were used: dodecyltrimethylammonium bromide, DTAB, with molecular weight $M_w$ = 308.34 Da - a cationic surfactant; sodium dodecyl sulfate (SDS) with molecular weight $M_w$ = 288.38 Da - an anionic surfactant (both obtained from Sigma Aldrich); Pantene shampoo which primarily consists of sodium lauryl sulfate; tetraethylene glycol monooctyl ether ($C_8E_4$) with molecular weight $M_w$ = 306.44 Da – a nonionic surfactant (obtained from Sigma Aldrich). In addition, a nonionic surfactant, Pluronic P-123 with molecular weight $M_w$ = 5750 Da, obtained from BASF Corporation was used.

**Solution Preparation.** DTAB, a cationic surfactant, SDS, an anionic surfactant, and $C_8E_4$, a nonionic surfactant were used to prepare solutions as follows. Using DTAB, 3.5 mM, 5 mM, 10 mM, 12 mM, 15 mM, 18 mM, and 20 mM aqueous solutions were prepared and denoted D3.5, D5.0, D10.0, D12.0, D15.0, D18.0, and D20.0, respectively. Using SDS, 2 mM, 4 mM, 6 mM, 8 mM, and 10 mM aqueous solutions were prepared and denoted SD2.0, SD4.0, SD6.0, SD8.0, and SD10.0, respectively. Using $C_8E_4$, 0.1 mM, 0.5 mM, 1 mM, 7.5 mM, and 10 mM aqueous solutions were prepared and denoted C0.1, C0.5, C1.0, C7.5, and C10.0, respectively. The surfactant concentrations used for preparing the solutions were both below and above the critical micelle concentration, which is 15 mM for DTAB,[31] 8 mM for SDS,[32,33] and 7.5 mM for $C_8E_4$.[24] For nonionic surfactant Pluronic P-123, a 1 mM aqueous solution was initially prepared and then diluted to 0.5 mM, 0.1 mM, and 0.052 mM and denoted as P0.5, P0.1, and P0.052, respectively. The critical micelle concentration of Pluronic P-123 is 0.052 mM at 25 °C.[34] Pantene soap solution was prepared by adding 5.0 mL of Pantene shampoo to 100 mL of deionized water. This solution was named PS5.0 and used only to form spherical soap bubbles.

**Experimental Setup.** The schematic of the experimental setup in which drainage from plane foam films was studied is shown in Figure 1. The light source used was Rayovac 145 lm white light. The light was kept at the focal length of a plano convex lens ($f$ = 12.5 cm) which produced parallel beam of light. To obtain a uniform parallel white light, Lumiquest diffuser was used.

A thin aluminum wire (4 cm × 4 cm × 0.087 cm) was used to withdraw and support plane soap films. The frame was fixed on a vertical black surface as shown in Figure 1 in such a way that it could be dipped into solutions in the container. The solutions were placed in a 100 mL beaker supported on a flange attached to a linear actuator. The beaker was initially raised to dip the frame completely into the solution in the container and then lowered using the linear actuator connected to a stand. The speed of the actuator was controlled with a 12 V dc supply. The frame with a film on it was fully withdrawn from the container and did not have any direct contact with the solution bulk throughout the entire experiment. The background of the frame was completely black to prevent any unwanted reflections from the surroundings. The film on the frame was photographed using a CCD camera (Phantom Miro 4), and the data were stored in the computer. Once the beaker was lowered, the camera was triggered. The withdrawal velocities of the frame were in the range 0.67–2.17 cm/s. The initial film thicknesses in this range practically did not change with withdrawal velocity. For example, for D10.0 films the initial film thickness at the top $h_0$ varied in the range 4006–4043 nm, and at the bottom the initial thickness $h_{bi}$ was in the range 4360–4389 nm. Therefore, the gravitational drainage time practically did not depend on the withdrawal velocity.

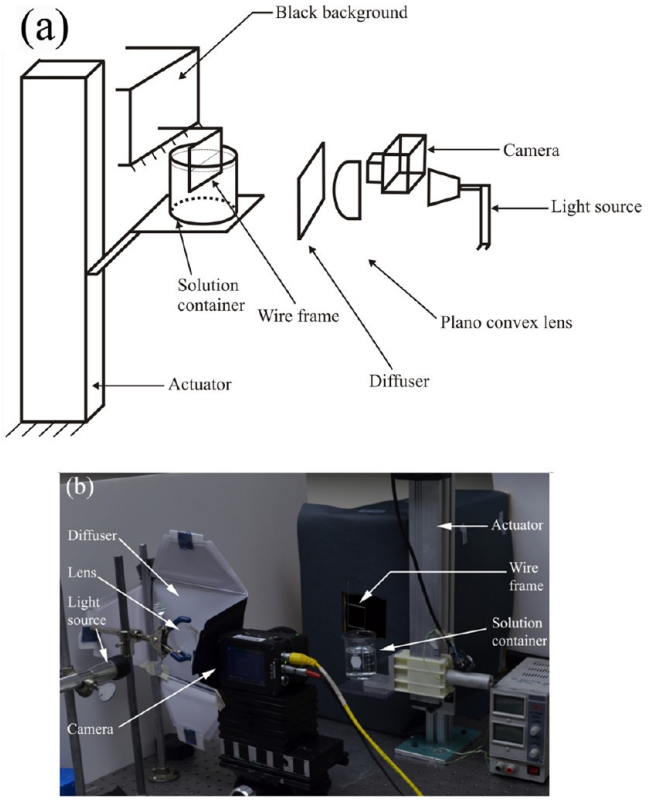


**Figure 1.** (a) Schematic of the experimental setup with drainage from plane films. (b) Image of the experimental setup.

The schematic of the experimental setup with drainage from spherical bubbles is shown in Figure 2. The light source, the plano convex lens, and diffuser were the same as those used for the plane film. A small container having the base diameter of 4.5 cm and a height of 3 cm was used. The solution was filled to the brim of the container. The container was completely black in color to reduce any unwanted reflections from its walls. A 5 $cm^3$ syringe was cut to make its length equal to the container height and fixed to its bottom at the center. The cut edge was smoothened to minimize any perturbations. A single 1 $cm^3$ bubble released at the liquid surface in the container at the center of the "fence" created by the cut 5 $cm^3$ syringe stayed at the same location during the entire observation time. The bubble was photographed using a CCD camera (Phantom Miro 4), and the data were stored in the computer.

**Experimental Method.** Using color images with white light sources are preferable than using monochromatic light.[35] A monochromatic light source produces alternate bands of dark and bright fringes. However, when using white light as in the present case, black bands appear only when the film thickness is small compared to the shortest visible wavelength. So, the black film provides a good reference point in determining the order of the color bands in the film as discussed below.

All films were mobile rather than rigid following terminology of ref 36, and correspondingly the duration of the drainage process was on the scale of 100 s (cf. Figure 3). In plane films the film thickness at the top was measured right below the top wire and 2 cm from the left wire, which is halfway across the frame. So the side wires did not have any effect on the film thickness. The film thickness was practically homogeneous horizontally across the wire frame. This is corroborated by the fact that the interference color bands were uniformly colored horizontally at any location along the $x$-axis (vertical) at any time (Figures 3a-3e). The different interference color bands in these figures


dx.doi.org/10.1021/la4003127 | Langmuir 2013, 29, 4934–4947

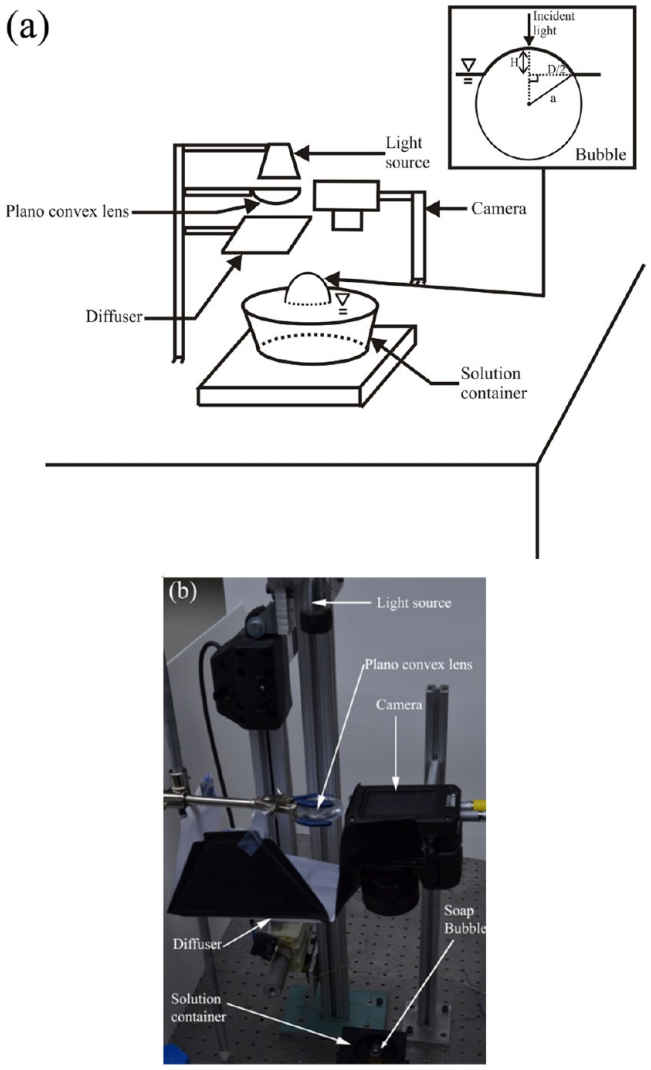


**Figure 2.** (a) Schematic of the experimental setup with drainage of spherical soap bubble. (b) Image of the experimental setup.

show that the film thickness varies in the vertical direction but is uniform in the horizontal direction.

The background image (with no film) shown in Figure 4a was subtracted from the film image shown in Figure 4b using MATLAB R-2011a. Then, each resulting color image (Figure 4c) was analyzed using MATLAB R-2011a. Each pixel in such a color image was mapped as a vector of three intensity components, i.e. $I(x,y) = \{I_r(x, y), I_g(x, y), I_b(x, y)\}$, where $I_r$, $I_g$, and $I_b$ refer to the red, green, and blue light components, respectively, with the wavelengths $\lambda$ = 650 nm for red, $\lambda$ = 500 nm for green, and $\lambda$ = 450 nm for blue light. In other words, the digital light filtering[18] was applied to the images produced by a single light source, and three different monochromatic light wavelengths corresponding to the red, green, and blue light were used independently in comparison.

For each wavelength of the red, green, and blue light, the local film thickness $h$ was calculated using the following interferometric formula[17−20,23] corresponding to either $I = I_r$, $I_g$, or $I_b$

$$h = \frac{\lambda_i}{2\pi n}\left[m\pi \pm \arcsin\sqrt{\frac{\Delta_i(1 + r^2)^2}{(1 - r^2)^2 + 4r^2\Delta_i}}\right] \quad (1)$$

where $\Delta_i = (I_i - I_{min,i})/(I_{max,i} - I_{min,i})$; $I_i$ is the instantaneous intensity corresponding to the wavelength $\lambda_i$ (i stands for either red, green, or blue light), and $I_{min,i}$ and $I_{max,i}$ are the minimum and maximum intensities, respectively, which were found using image analysis software developed on the platform of MATLAB R-2011a. In addition, $r$ is the Fresnel's reflection coefficient given by $r = (n - 1)/(n + 1)$ for the normal incident light, with $n$ being the refractive index of the film liquid (water), $m$ is the order of interference, $m$ = 0,1,2.... The refractive index for soap water in air films was taken as $n$ = 1.333.

When a film bursts near the top wire, the light intensity from that area is minimal, i.e. $\Delta_i = 0$. On the other hand, the film thickness is also zero, which means that according to eq 1 one should assign $m = 0$ to the top part of the film at the moment of bursting. Tracing the recorded light intensity at the film top back in time from the moment of bursting, one has to increase $m$ by 1 and change the plus sign by the minus sign each time $\arcsin\ (\Delta_i(1 + r^2)^2/[(1 - r^2)^2 + 4r^2\Delta_i])^{1/2}$ becomes equal to $\pi/2$ after increasing from 0 (when the plus sign was used). This allows one to establish the values of $m$ at the film top at any time. Then, for any instantaneous intensity pattern, the value of $m$ is increased by 1 in moving from the film top when the value of the arcsine becomes zero.

It was found that for the film thicknesses above 30 nm the results obtained using different wavelengths corroborated each other and were identical, as is seen in Figure 5. The figure shows that the

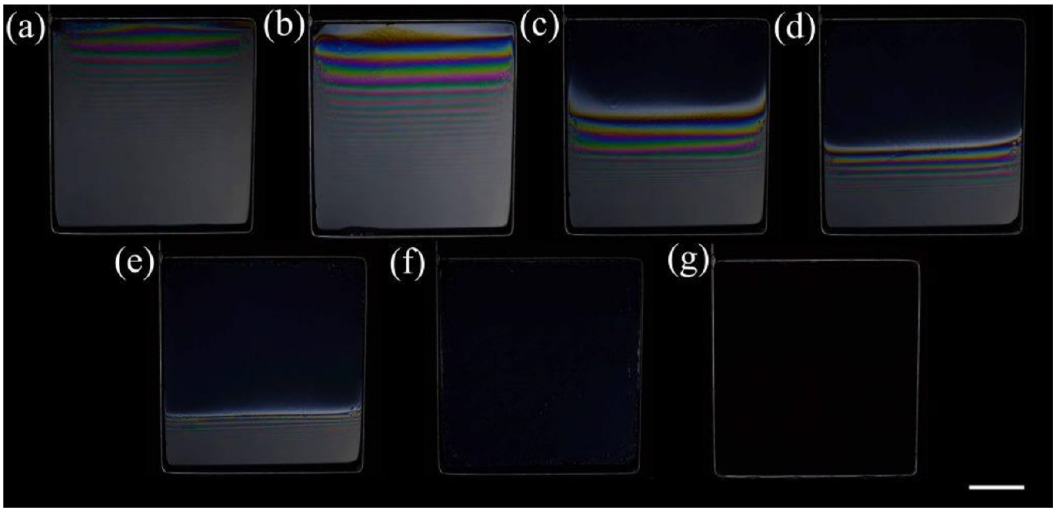


**Figure 3.** Drainage of D10.0 plane film. Interference pattern at (a) $t$ = 25 s, (b) $t$ = 50 s, (c) $t$ = 60 s, (d) $t$ = 70 s, and (e) $t$ = 80 s. The formation of the black film can be seen at the top at (b) $t$ = 50 s. After that the lower boundary of the black film is advancing downward until the entire film becomes black at (f) $t$ = 90 s. The film explodes at (g) $t$ = 98 s. The scale bar is 1 cm.


dx.doi.org/10.1021/la4003127 | Langmuir 2013, 29, 4934−4947

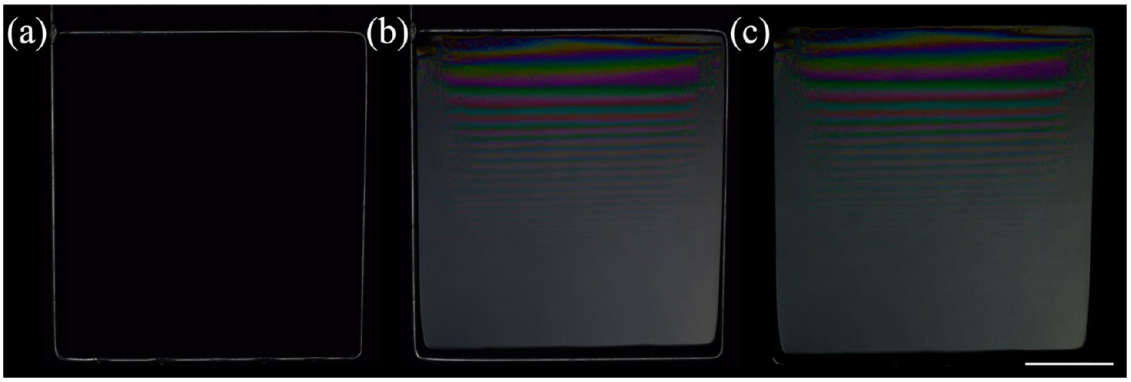


**Figure 4.** (a) The image of an empty wire frame against the black background. (b) Color image of the frame with a film against the black background. (c) The film image with the wire frame and background subtracted. The scale bar is 1 cm.

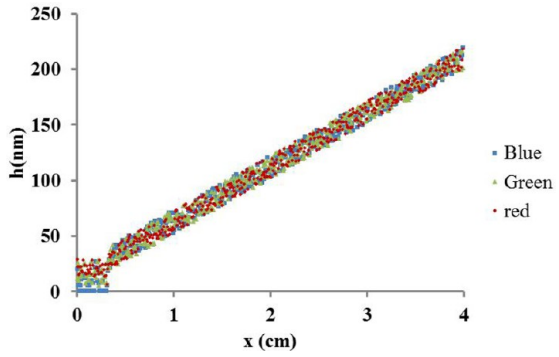


**Figure 5.** Thickness of planar film measured using the intensities of red, green, and blue light, $I_r$, $I_g$, and $I_b$, respectively, filtered digitally. DTAB solution D10.0 film at $t$ = 70 s; $x$ = 0 corresponds to the topmost section of the film where the black film was formed.

accuracy of the film thickness measurements is about ±7 nm, and fully reliable and self-consistent data can be acquired for the film thicknesses above 30 nm. It is emphasized that to obtain accurate results, a background image was subtracted from each image containing soap film using MATLAB R-2011a. For planar films, the axis of the camera was always normal to the tangent plane of the film, making the incidence angle $\theta = 0°$ (cf. Figure 1). The film thickness was measured for the entire lifetime of planar films all over their lengths.

When a plane film adjoins a wire frame, the latter plays a role of the Plateau border, and capillary suction results in the flow component toward the wire. The film margins affected by such a flow can be subjected to the instability called marginal regeneration which is associated with the surfactant concentration-driven Marangoni effect.[32,36−40] The marginal regeneration is always clearly visible in the form of "balloons" and "mushrooms" departing from the wire, which are the manifestations of the film thickness variations in the color interferometric images. It is emphasized that the images in Figures 3 show that in the present experiments with relatively thick films with mobile surfaces no signs of marginal regeneration were visible on the plane films. They were unaffected by the marginal instability probably because the gravity-driven flow dominated the capillary suction to the horizontal wires in the frame.

In the case of bubbles in the setup in Figure 2, the analysis of the images (Figure 6) revealed that the bubble surface was perfectly spherical, and its radius of curvature can be expressed as $a = H/2 + D^2/8H$ (see the inset in Figure 2a). However, unlike the planar films, the spherical bubble could not be imaged from the side because the incident light angle changed constantly due to the change of the normal projected from the film surface, which made measurements of the film thickness inaccurate. As a result, the film thickness along the entire height of the bubble could not be measured. Therefore, in the experiments the light source and camera were kept directly above the bubble apex. Then, the film thickness at the apex of the bubble could be measured as the camera was parallel to the normal projected from the bubble surface at the apex, making the incidence angle $\theta = 0°$.

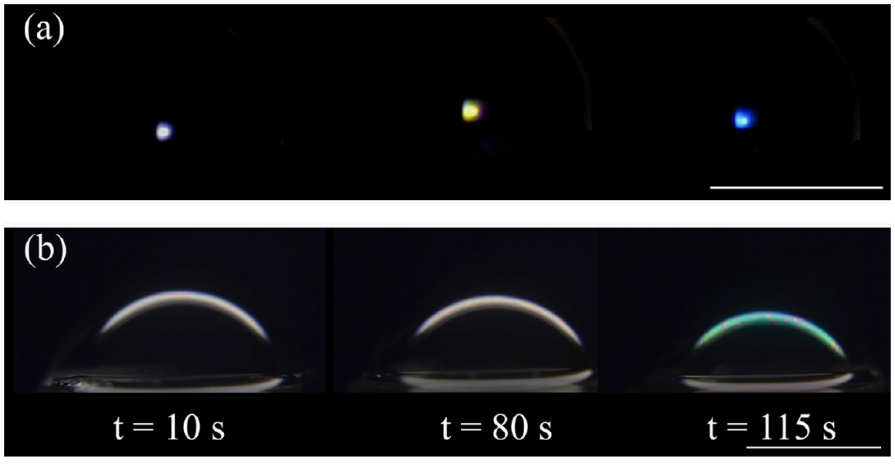


**Figure 6.** Drainage of D10.0 spherical bubble. The measurements of the film thickness at the bubble apex were done at different time moments using the interference color pattern seen in panel (a). (b) In a separate experiment, the side views for these moments were recorded. The scale bar is 1 cm for both sets of images.


dx.doi.org/10.1021/la4003127 | *Langmuir* 2013, 29, 4934−4947

## THEORETICAL

In the present section a theory of gravity-driven drainage from surfactant-stabilized liquid films is developed. The theory describes stretching of the upper part of the film by the weight of the lower one. As a result of such stretching, concentration of surfactant molecules at the surface in the upper part of the film decreases compared to the lower one. Accordingly, surface tension in the upper part of the film increases compared to the lower one, and the associated concentration-driven Marangoni flow directed upward arises. This flow tends to diminish drainage and is identical to the surface elasticity, which decelerates gravity-driven drainage.

**Drainage of Plane Soap Film.** Consider a vertical plane soap film suspended on a wide rectangular wire frame sketched in Figure 7. Denote the coordinate reckoned in the drainage direction as $x$ and the coordinate normal to it as $y$.

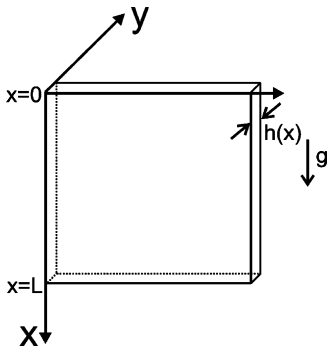


**Figure 7.** Sketch of vertical plane soap film on a frame.

As discussed below, quasi-one-dimensional approximation can be adopted to describe drainage of such films. Namely, the continuity equation reads

$$\frac{\partial h}{\partial t} + \frac{\partial uh}{\partial x} = 0 \tag{2}$$

where the film thickness is denoted as $h$, the longitudinal velocity as $u$, and time as $t$.

The drainage flow is relatively slow, which allows one to neglect the inertial effects. The normal viscous stresses in the film are also negligible. However, at the film surface acts shear stress $\sigma_{yx,surf}$. This stress appears due to a possible nonuniform distribution of surfactant at the film surface, i.e. due to the concentration Marangoni effect.[4,6,7] The corresponding longitudinal momentum balance reads

$$\sigma_{yx,surf} = -\frac{\rho g h}{2} \tag{3}$$

where $\rho$ is the liquid density, and $g$ is the gravity acceleration. It is emphasized that a uniform surface tension does not contribute to this equation because in the case of a film surface practically aligned with the $x$-axis, it equally pulls any film element in the opposite sides. Only, if the film is cut, surface tension being unbalanced at the cut line can produce fluid motion in the form of a moving and growing free rim causing the Taylor-Culick retraction.[41,42] It is emphasized that eq 3 in ref 26 can be rearranged to our eq 3.

This shear stress is transmitted into the film bulk by viscous shear stresses, which tend to equilibrate the surface and bulk velocity. Such equilibration takes place at the distances of the order $\delta = \mu u/(\rho g h)$. With the characteristic values of the parameters corresponding to the present experiments ($\mu/\rho = 10^{-2}$ cm$^2$/s, $u = 10^{-2}$ cm/s, and $h = 10^{-4}$ cm), the value of $\delta$ is of the order of $\delta = 10^{-3}$ cm, which is larger than the film thickness $h$. This makes the velocity profile in the $y$-direction practically uniform, and thus the quasi-one-dimensional approximation $u = u(x,t)$ possible.

On the other hand, the shear stress $\sigma_{yx,surf}$ is determined by the surface elasticity $\varepsilon$ of soap films, which is associated with the concentration Marangoni effect.[4,6,7] The corresponding surface elasticity (the Gibbs elasticity[7,17]) $\varepsilon = -\Gamma(\partial\sigma/\partial\Gamma)$ is associated with the dependence of the surface tension $\sigma$ on the distribution of surfactant concentration $\Gamma$ at the surface. If one follows a material surface element with an initial coordinate $\xi$ which will be used as a Lagrangian parameter, stretching of the element can be expressed as $\partial l/\partial\xi$ where $d\xi$ is the initial length of the element and $dl$ is its current length. The elastic energy of a surface element with a unit width is then given by $dU = \varepsilon(\partial l/\partial\xi)d\xi$, which implies that no surfactant adsorption/desorption takes place at the surface during the experiment in agreement with the estimates in ref 7. In the expression for $dU$ only the linear term of the expansion in strain is accounted for with $\varepsilon$ being a constant, which formally corresponds to small strains and linear elastic response. As usual in the phenomenological approach to rheology, if dictated by an experimental evidence, generalizations to a nonlinear elastic response could be done similarly to the nonlinear theory of elasticity.[43] The elastic force $dF = \partial(dU)/\partial\xi$, and correspondingly, $\sigma_{yx,surf} = dF/dS = \varepsilon\partial^2 l/\partial\xi^2$, where the area of an element of the unit width $dS = d\xi$. Then, eq 3 can be transformed to the following form

$$-\frac{\rho g h}{2} = \varepsilon\frac{\partial^2 l}{\partial\xi^2} \tag{4}$$

The kinematic relation

$$\frac{d}{dt}\left(\frac{\partial l}{\partial\xi}\right) = \frac{\partial u}{\partial\xi} \tag{5}$$

allows one to transform the momentum balance eq 4 to the following form

$$-\frac{\rho g}{2\varepsilon}\frac{dh}{dt} = \frac{\partial^2 u}{\partial x^2} \tag{6}$$

The latter can be rewritten as

$$\frac{\partial h}{\partial t} + u\frac{\partial h}{\partial x} = -\frac{2\varepsilon}{\rho g}\frac{\partial^2 u}{\partial x^2} \tag{7}$$

It is emphasized that eqs 6 and 7 can be also derived using as a starting point the equation of surfactant balance at the interface

$$\frac{\partial\Gamma}{\partial t} + \frac{\partial\Gamma u}{\partial x} = 0 \tag{8}$$

together with the momentum balance eq 3 and the kinematic relation eq 5.

Note also, that eq 8 disregards adsorption or desorption of surfactant molecules at the film surface during the drainage process, which lasts of the order of 50−100 s. Since both the bulk and surface liquid elements are equally stretched when a film is formed, the concentration gradient across the film is negligible, while surfactant molecules can be delivered to a depleted section of the surface only along the film. The


dx.doi.org/10.1021/la4003127 | Langmuir 2013, 29, 4934−4947

characteristic times of the bulk and surface diffusion along the film are $\tau_{Db} \approx a^2/D_b$ and $\tau_{Ds} \approx a^2/D_s$, respectively, where $D_b$ and $D_s$ denote the bulk and surface diffusion coefficients, respectively, and $a$ is of the order of the wire diameter. Taking for the estimate $D_b \approx 10^{-5}$ cm$^2$/s and $D_s \approx 10^{-7}$ cm$^2$/s as in ref 7, we find that in the present case $\tau_{Db} \approx 10^3$ s and $\tau_{Ds} \approx 10^5$ s, much longer than the drainage process, indeed.

Combining eqs 2 and 7, we obtain the following expression for the film thickness $h$

$$h = \frac{2\varepsilon}{\rho g}\frac{\partial^2 u/\partial x^2}{\partial u/\partial x} \tag{9}$$

Integrating eq 2 from the top of the film at $x = 0$, we recast the continuity equation to the following form

$$\frac{\partial}{\partial t}\int_0^x h\mathrm{d}x + uh = 0 \tag{10}$$

Substituting eq 9 into eq 10, we obtain the following equation for $u$

$$\frac{\partial^2 u}{\partial t \partial x} + u\frac{\partial^2 u}{\partial x^2} = 0 \tag{11}$$

The latter can be expressed as the system of two equations of the first order

$$\frac{\partial f}{\partial t} + u\frac{\partial f}{\partial x} = 0 \tag{12}$$

$$f = \frac{\partial u}{\partial x} \tag{13}$$

Our problem on the film drainage involves four physical parameters: liquid density $\rho$, gravity acceleration $g$, surface elasticity $\varepsilon$, and the characteristic film thickness, say, the initial thickness at the film top $h_0$. Two time scales can be constructed from these physical parameters

$$T = \frac{\varepsilon}{\rho(gh_0)^{3/2}} \tag{14}$$

and

$$\tau_g = \left(\frac{h_0}{g}\right)^{1/2} \tag{15}$$

The time scale $T$ is related to the surface elasticity $\varepsilon$ and is definitely relevant for the drainage process. The time scale $\tau_g$ does not depend on the surface elasticity and thus is irrelevant. Indeed, taking for the estimate $h_0 = 1$ $\mu$m, we find $\tau_g \sim 1$ ms, whereas the duration of drainage from plane films is of the order of 50−100 s. Moreover, the viscous time scale (if one assumes that viscosity $\mu$ plays any role), $\tau_\mu = \mu/(\rho g h_0)$, is also incommensurate with the duration of the drainage process, since $\tau_\mu \sim 0.1$ s. Therefore, the model of drainage assuming rigid film surfaces with the viscous friction-determined parabolic velocity profile of drainage flow[37] is inapplicable in the present case.

Render eqs 9, 12, and 13 dimensionless using $T$ as the scale of $t$, $h_0$ as the scale of $x$ and $h$, $h_0/T$ as the scale of $u$, and $T^{-1}$ as the scale of $f$. Then, these equations take the following dimensionless form

$$\overline{h} = E\frac{\partial^2 \overline{u}/\partial \overline{x}^2}{\partial \overline{u}/\partial \overline{x}} \tag{16}$$

$$\frac{\partial \overline{f}}{\partial \overline{t}} + \overline{u}\frac{\partial \overline{f}}{\partial \overline{x}} = 0 \tag{17}$$

$$\overline{f} = \frac{\partial \overline{u}}{\partial \overline{x}} \tag{18}$$

In eq 16 the dimensionless group $E$ is given by

$$E = \frac{2\varepsilon}{\rho g h_0^2} \tag{19}$$

The hyperbolic eq 17 is solved by the method of characteristics, and the solution reads

$$\overline{f} = \psi'(\xi) \tag{20}$$

$$\overline{x} = \xi + \int_0^{\overline{t}} \overline{u}\,\mathrm{d}\overline{t} \tag{21}$$

where $\xi$ is the $\overline{x}$-coordinate of an individual fluid element at $\overline{t} = 0$, and prime denotes the first derivative in $\xi$. It is emphasized that eq 20 means that $\partial u/\partial x = \partial u/\partial \xi$ on a material element, which was implied in eq 6.

At $\overline{t} = 0$ the initial thickness distribution is known and given as $\overline{h} = \overline{h_0}\ (\xi)$. On the other hand, according to eqs 16 and 18, $\overline{h_0}\ (\xi) = E(\mathrm{d}\overline{f}/\mathrm{d}\xi)/\overline{f}$. Therefore, using eq 20, we find

$$\overline{f}\ (\xi) = \psi'(\xi) = \exp\left[\frac{1}{E}\int \overline{h_0}(\xi)\mathrm{d}\xi\right] \tag{22}$$

and, in principle, the function $\psi(\xi)$ is established.

From eq 21 we find

$$1 = \frac{\partial \xi}{\partial \overline{x}} + \int_0^{\overline{t}} \frac{\partial \overline{u}}{\partial \overline{x}}\mathrm{d}\overline{t} \approx \frac{\partial \xi}{\partial \overline{x}} + \int_0^{\overline{t}} \psi'\mathrm{d}\overline{t} = \frac{\partial \xi}{\partial \overline{x}} + \psi'\overline{t} \tag{23}$$

It is emphasized that the approximate equality in eq 22 corresponds to the limit of small values of $\overline{t}$ (which will not be too restrictive, as the comparison with the experiments shows below) and involves the usage of eqs 18 and 20. Therefore, from eq 23 we find

$$\frac{\partial \xi}{\partial \overline{x}} = 1 - \psi'\overline{t} \tag{24}$$

Then, from eqs 16, 18, 20, and 24 we find

$$\overline{h} = E\frac{\psi''(1 - \overline{t}\psi')}{\psi'} \tag{25}$$

Substituting eq 22 into eq 25, we arrive at

$$\overline{h}(\overline{x}, \overline{t}) = \overline{h_0}(\xi)\left\{1 - \overline{t}\exp\left[\frac{1}{E}\int \overline{h_0}(\xi)\mathrm{d}\xi\right]\right\} \tag{26}$$

$$\overline{x} = \int_0^{\xi} \frac{\mathrm{d}\xi}{1 - \overline{t}\exp[E^{-1}\int \overline{h_0}(\xi)\mathrm{d}\xi]} \tag{27}$$

At small $\xi$, i.e. close to the top of the film, we can find from eqs 26 and 27

$$\overline{h}(\overline{x}, \overline{t}) = (1 - \overline{t})\exp\left(-\frac{\overline{x}\,\overline{t}}{E}\right) \tag{28}$$

Therefore, at small $\overline{x}$ close to the film top, $\overline{h}\ (\overline{x}, \overline{t}) \approx (1 - \overline{t})$, and thus the dimensional expression for the thickness at small $x$ and $t$ reads


dx.doi.org/10.1021/la4003127 | Langmuir 2013, 29, 4934−4947

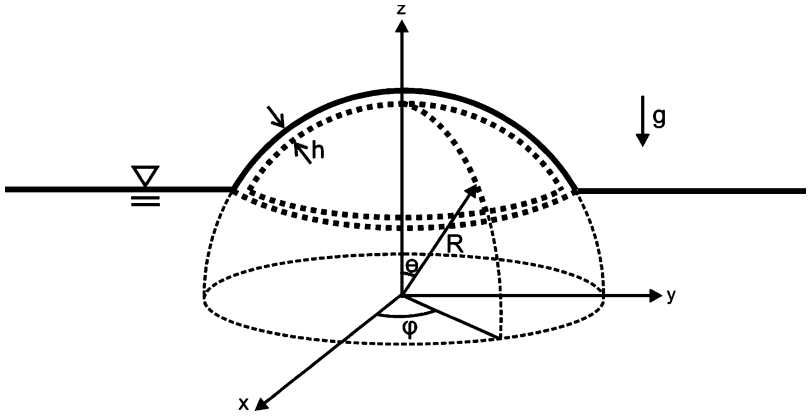


**Figure 8.** Sketch of spherical soap film. $R$ denotes the bubble radius.

$$h(x, t) = h_0\left(1 - \frac{t}{T}\right) \tag{29}$$

It shows that close to the top of the film it is expected to rupture at the time moment $t = T$. That will be measured experimentally (see below) and thus reveal the value of the film elasticity with the help of eq 14.

**Drainage of Spherical Soap Bubble.** Spherical soap bubble is sketched in Figure 8. The continuity equation which replaces eq 2 of the plane film and expresses the mass balance in the case of drainage from a spherical film takes the following form

$$\frac{\partial h}{\partial t} + \frac{1}{R \sin\theta}\frac{\partial h v_\theta \sin\theta}{\partial \theta} = 0 \tag{30}$$

where $v_\theta$ is the flow velocity along the generatrix.

The momentum balance equation which replaces eq 3 of the plane film in the case of drainage from a spherical film reads

$$\sigma_{r\theta,\mathrm{surf}} = -\frac{\rho g h}{2}\sin\theta \tag{31}$$

The uniform surface tension cannot contribute to eq 31 by the same reason as explained in relation to eq 3.

In the case of spherical films, a material element experiences biaxial strain, with the principal strains being

$$\omega_{\theta\theta} = \frac{\partial l}{\partial \xi},\ \omega_{\varphi\varphi} = \frac{\sin\theta}{\sin\alpha} \tag{32}$$

which correspond to the two angular spherical coordinates $\theta$ and $\varphi$ (cf. Figure 8), and $\alpha$ being an initial value of the angular coordinate $\theta$ for an element (its Lagrangian parameter), with $\xi = R\alpha$.

The corresponding elastic energy of a material element of the film is

$$\mathrm{d}U = \varepsilon(\omega_{\theta\theta} + \omega_{\varphi\varphi})\mathrm{d}\xi 2\pi R \sin\theta \tag{33}$$

which implies that no surfactant adsorption/desorption takes place at the surface during the experiment following the estimates of ref 7. The elastic force $\mathrm{d}F = \partial(\mathrm{d}U)/\partial\xi$ and, correspondingly, the shear stress at the film surface

$$\begin{aligned}\sigma_{r\theta,\mathrm{surf}} &= \frac{\mathrm{d}F}{\mathrm{d}S} \\ &= \frac{\mathrm{d}F}{2\pi R \sin\alpha \mathrm{d}\xi} \\ &= \frac{\varepsilon}{\sin\alpha}\frac{\partial}{\partial\xi}[\sin\theta(\omega_{\theta\theta} + \omega_{\varphi\varphi})]\end{aligned} \tag{34}$$

where $\mathrm{d}S$ is the element surface area.

Then, eqs 31 and 34 yield

$$-\frac{\rho g h}{2}\sin\theta = \frac{\varepsilon}{\sin\alpha}\frac{\partial}{\partial\xi}[\sin\theta(\omega_{\theta\theta} + \omega_{\varphi\varphi})] \tag{35}$$

The kinematic relations associated with time differentiation, which follow from eq 32 read

$$\begin{aligned}\frac{\mathrm{d}\omega_{\theta\theta}}{\mathrm{d}t} &= \frac{\mathrm{d}}{\mathrm{d}t}\left(\frac{\partial l}{\partial\xi}\right) = \frac{\partial v_\theta}{R\partial\theta}, \\ \frac{\mathrm{d}\omega_{\varphi\varphi}}{\mathrm{d}t} &= \frac{\cos\theta}{\sin\alpha}\frac{\mathrm{d}\theta}{\mathrm{d}t} = \frac{\cos\theta}{\sin\alpha}\frac{v_\theta}{R}\end{aligned} \tag{36}$$

Then, eqs 35 and 36 yield

$$-\frac{\rho g}{2\varepsilon}\frac{\mathrm{d}h}{\mathrm{d}t} = \frac{1}{R\sin\theta}\frac{\partial}{\partial\theta}\left[\frac{1}{R\sin\theta}\frac{\partial(v_\theta\sin\theta)}{\partial\theta}\right] \tag{37}$$

The latter equation can also be derived using the equation which governs surfactant concentration at the film surface in the spherical case

$$\frac{\partial\Gamma}{\partial t} + \frac{1}{R\sin\theta}\frac{\partial\Gamma v_\theta \sin\theta}{\partial\theta} = 0 \tag{38}$$

which replaces eq 8 of the planar case.

In the Eulerian framework eq 37 takes the following form

$$\frac{\partial h}{\partial t} + \frac{v_\theta}{R}\frac{\partial h}{\partial\theta} = -\frac{2\varepsilon}{\rho g R\sin\theta}\frac{\partial}{\partial\theta}\left[\frac{1}{R\sin\theta}\frac{\partial}{\partial\theta}(v_\theta\sin\theta)\right] \tag{39}$$

which replaces eq 7 of the planar case.

The latter equation in combination with the continuity eq 30 yields the following expression for the film thickness $h$

$$h = \frac{2\varepsilon}{\rho g}\frac{\partial}{\partial\theta}\left[\frac{1}{R\sin\theta}\frac{\partial(v_\theta\sin\theta)}{\partial\theta}\right]\Big/\frac{\partial(v_\theta\sin\theta)}{\partial\theta} \tag{40}$$

In the case of drainage from spherical films this equation replaces eq 9.


dx.doi.org/10.1021/la4003127 | Langmuir 2013, 29, 4934−4947

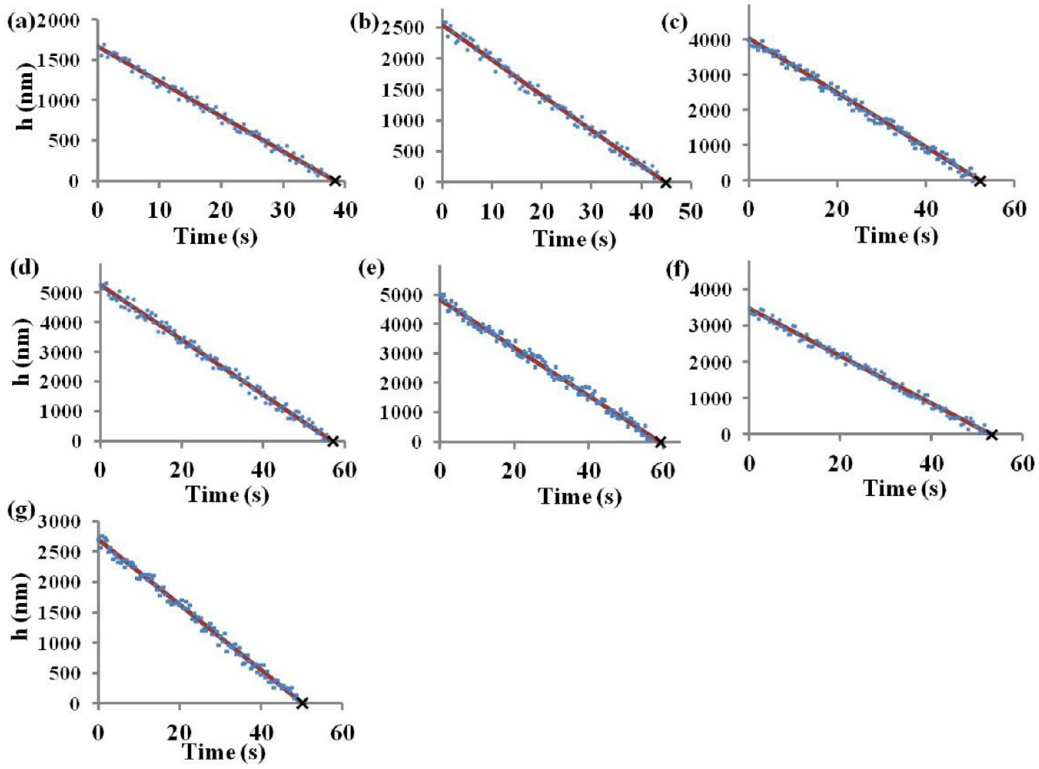


**Figure 9.** Drainage of DTAB solution films: (a) D3.5, (b) D5.0, (c) D10.0, (d) D12.0, (e) D15.0, (f) D18.0, and (g) D20.0. The data correspond to the film top. The experimental results are shown by symbols. The inclined straight lines correspond to the theoretical result, eq 29.

Using eqs 30 and 40, one derives the following equation for $v_\theta$

$$\frac{\partial^2(v_\theta \sin\theta)}{\partial\zeta\partial t} + \frac{v_\theta \sin\theta}{R}\frac{\partial^2(v_\theta \sin\theta)}{\partial\zeta^2} = 0 \tag{41}$$

where $\zeta = -\cos\theta$. This equation is a spherical counterpart of eq 11.

Equation 40 is equivalent to the following system of two equations of the first order

$$\frac{\partial f}{\partial t} + \frac{v_\theta}{R}\frac{\partial f}{\partial\theta} = 0 \tag{42}$$

$$f = \frac{1}{\sin\theta}\frac{\partial(v_\theta \sin\theta)}{\partial\theta} \tag{43}$$

which replace eqs 12 and 13 of the planar case.

Render $v_\theta$ and $f$ by $R/T$, and time $t$ by $T$. Then, eqs 40, 42, and 43 take the following dimensionless form

$$\overline{h} = \frac{h_0}{R}E\frac{\partial}{\partial\theta}\left[\frac{1}{\sin\theta}\frac{\partial(\overline{v}_\theta \sin\theta)}{\partial\theta}\right] \Big/ \frac{\partial(\overline{v}_\theta \sin\theta)}{\partial\theta} \tag{44}$$

$$\frac{\partial\overline{f}}{\partial\overline{t}} + \overline{v}_\theta\frac{\partial\overline{f}}{\partial\theta} = 0 \tag{45}$$

$$\overline{f} = \frac{1}{\sin\theta}\frac{\partial(\overline{v}_\theta \sin\theta)}{\partial\theta} \tag{46}$$

The approximate solution of eq 45 at small values of $\overline{t}$ is found similarly to the planar case as

$$\overline{f} = \overline{f(\xi)} = \psi'(\xi) = \exp\left[\frac{1}{(h_0/R)E}\int\overline{h_0(\xi)}\sin\xi\,\mathrm{d}\xi\right] \tag{47}$$

which replaces eq 22.

Then, eq 44 yields

$$\overline{h} = \overline{h_0(\xi)}[1 - \overline{v_\theta'(\xi)}\overline{t}\,] \tag{48}$$

while from eq 46 it follows that

$$\frac{\mathrm{d}\overline{v}_\theta}{\mathrm{d}\xi} = \frac{\mathrm{d}}{\mathrm{d}\xi}\left[\frac{1}{\sin\xi}\int\psi'(\xi)\sin\xi\,\mathrm{d}\xi\right] \tag{49}$$

At small $\xi$ close to the bubble apex, $\psi'(\xi) \approx 1$, and according to eq 49, $v_\theta'(\xi) \approx 1/2$ . Therefore, at small $\overline{t}$ and $\xi$ the film thickness given by eq 48 reduces to

$$\overline{h} = \overline{h_0(\xi)}\left(1 - \frac{\overline{t}}{2}\right) \tag{50}$$

The dimensional form of eq 50 reads

$$h(x, t) = h_0\left(1 - \frac{t}{2T}\right) \tag{51}$$

This equation shows that drainage from spherical films is slower than drainage from plane films described by eq 29. This stems from the fact that the effect of the driving force, gravity, on the flow is stronger in the plane films, since they are oriented vertically, whereas the spherical films are inclined at the most part of their generatrix.

## RESULTS AND DISCUSSION

**Drainage of Plane Soap Film.** Solutions with different concentrations of the cationic surfactant DTAB and the anionic


dx.doi.org/10.1021/la4003127 | Langmuir 2013, 29, 4934−4947

**Table 1. Plane DTAB Solution Films**[a]

| sol. | $t$ (s) | $t_b$ (s) | $x$ (cm) | $t_{be}$ (s) | $h_i = h_0$ (nm) | $h_{bi}$ (nm) | $T$ (s) | $\varepsilon$ (g/s$^2$) |
|---|---|---|---|---|---|---|---|---|
| D3.5 | 63 | 38 | 2.6 | - | 1650.75 | 1853.56 | 38.37 | 2.49 |
| D5.0 | 73 | 44 | 2.9 | - | 2601.92 | 2930.96 | 44.89 | 5.78 |
| D10.0 | 98 | 51 | 4 | 90 | 4013.32 | 4388.94 | 52.17 | 12.87 |
| D12.0 | 117 | 55 | 4 | 106 | 5267.63 | 5652.14 | 55.91 | 20.74 |
| D15.0 | 124 | 58 | 4 | 111 | 4995.81 | 5109.52 | 59.16 | 20.27 |
| D18.0 | 120 | 52 | 4 | 101 | 3488.66 | 3859.41 | 53.04 | 10.60 |
| D20.0 | 105 | 49 | 4 | 92 | 2710.35 | 2998.82 | 50.13 | 6.86 |

[a]The film lifetime is denoted $t$; $t_b$ denotes the time at which black film sets in at the top of the wire frame; $t_{be}$ denotes the time at which black film covers the entire wire frame. The $x$ column corresponds to the position in the film (reckoned from the top) to which the leading edge of the black film reached at the moment of bursting. The initial film thickness at the top is denoted $h_i = h_0$, and at the bottom - $h_{bi}$; the drainage time $-T$. The values of the surface elasticity $\varepsilon$ were found from $T$ using eq 14.

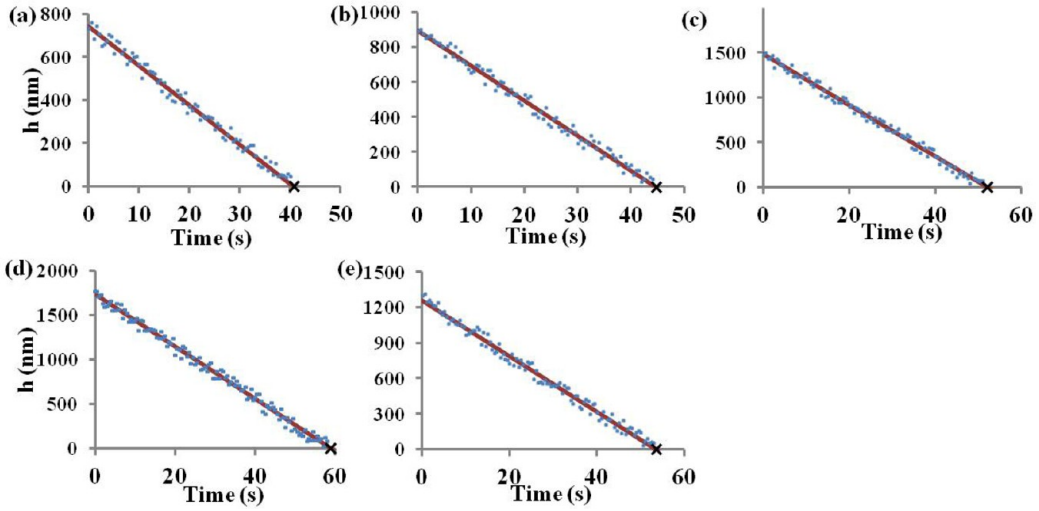


**Figure 10.** Drainage of SDS solution films: (a) SD2.0, (b) SD4.0, (c) SD6.0, (d) SD8.0, and (e) SD10.0. The data correspond to the film top. The experimental results are shown by symbols. The inclined straight lines correspond to the theoretical result, eq 29.

**Table 2. Plane SDS Solution Films**[a]

| sol. | $t$ (s) | $t_b$ (s) | $x$ (cm) | $t_{be}$ (s) | $h_i = h_0$ (nm) | $h_{bi}$ (nm) | $T$ (s) | $\varepsilon$ (g/s$^2$) |
|---|---|---|---|---|---|---|---|---|
| SD2.0 | 65 | 39 | 2.05 | - | 734.45 | 983.85 | 40.65 | 0.79 |
| SD4.0 | 79 | 44 | 3.8 | - | 892.71 | 1136.98 | 44.71 | 1.16 |
| SD6.0 | 102 | 51 | 4.0 | 98 | 1481.94 | 1796.88 | 51.96 | 2.88 |
| SD8.0 | 117 | 58 | 4.0 | 105 | 1770.29 | 1942.13 | 58.89 | 4.26 |
| SD10.0 | 104 | 53 | 4.0 | 97 | 1259.48 | 1548.37 | 53.52 | 2.32 |

[a]The film lifetime is denoted $t$; $t_b$ denotes the time at which black film sets in at the top of the wire frame; $t_{be}$ denotes the time at which black film covers the entire wire frame. The $x$ column corresponds to the position in the film (reckoned from the top) to which the leading edge of the black film reached at the moment of bursting. The initial film thickness at the top is denoted $h_i = h_0$, and at the bottom - $h_{bi}$; the drainage time $-T$. The values of the surface elasticity $\varepsilon$ were found from $T$ using eq 14.

surfactant SDS were used in experiments with drainage of the plane films. For DTAB solution D3.5, the top part of the plane film turned black (Figure 9a) and the black film advanced downward. The black film was present for about half the length of the film along the wire frame at the time of bursting. For DTAB solution D5.0 (Figure 9b) the black film reached further down the film at the instant of bursting, but the color bands were still seen at the bottom of the film. In the case of DTAB solution D10.0 (Figure 9c), the entire film turned black just before the instant of bursting. For DTAB solution D12.0 (Figure 9d), the entire film turned black and had a sufficient stability to last for about 60 s after the black film was formed before bursting.

The data in Figure 9 allow one to find the characteristic drainage time $T$ as the time moment when $h$ approaches zero, as follows from eq 29. The latter perfectly agrees with the experimental data. Then, eq 14 is used to find the corresponding values of the surface elasticity $\varepsilon$, since the other parameters in it are known. The results for the DTAB solutions are summarized in Table 1, where, in particular, the measured values of the film elasticity $\varepsilon$ are listed.

For the anionic SDS solutions SD2.0 to SD10.0 (Figures 10a-10e, respectively) similar trends were observed as those in Figure 9 for DTAB. In all the cases, black films were formed at the top and the films turned completely black for SD6.0, SD8.0, and SD10.0.

The values of the cutoff time $T$ were established using the experimental data in Figure 10. Then, the film elasticity $\varepsilon$ was calculated from eq 14. The results for the SDS solutions are


dx.doi.org/10.1021/la4003127 | Langmuir 2013, 29, 4934−4947

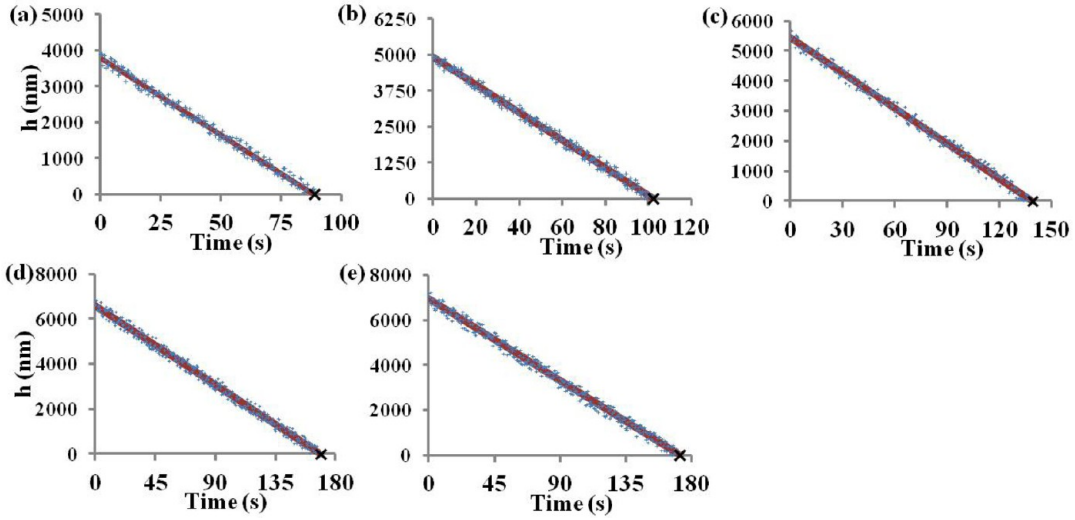


**Figure 11.** Drainage of $C_8E_4$ solution films: (a) C0.1, (b) C0.5, (c) C1.0, (d) C7.5, and (e) C10.0. The data correspond to the film top. The experimental results are shown by symbols. The inclined straight lines correspond to the theoretical result, eq 29.

**Table 3. Plane Films of the Nonionic $C_8E_4$ Solutions**[a]

| sol. | $t$ (s) | $t_b$ (s) | $x$ (cm) | $t_{be}$ (s) | $h_i = h_0$ (nm) | $h_{bi}$ (nm) | $T$ (s) | $\varepsilon$ (g/s$^2$) |
|---|---|---|---|---|---|---|---|---|
| C0.1 | 98 | 89 | 4 | 96 | 3761.62 | 4014.28 | 88.88 | 19.89 |
| C0.5 | 114 | 102 | 4 | 110 | 4896.28 | 5207.64 | 102.3 | 34.00 |
| C1.0 | 151 | 138 | 4 | 144 | 5432.91 | 5861.72 | 139 | 54.00 |
| C7.5 | 190 | 167 | 4 | 182 | 6617.34 | 6940.23 | 169.03 | 88.27 |
| C10 | 189 | 170 | 4 | 183 | 6943.55 | 7086.22 | 172.09 | 99.59 |

[a]The film lifetime is denoted $t$; $t_b$ denotes the time at which black film sets in at the top of the wire frame; $t_{be}$ denotes the time at which black film covers the entire wire frame. The $x$ column corresponds to the position in the film (reckoned from the top) to which the leading edge of the black film reached at the moment of bursting. The initial film thickness at the top is denoted $h_i = h_0$, and at the bottom - $h_{bi}$; the drainage time $-T$. The values of the surface elasticity $\varepsilon$ were found from $T$ using eq 14.

summarized in Table 2, where, in particular, the measured values of the film elasticity $\varepsilon$ are listed.

For the cationic and anionic surfactant solutions with concentrations below the corresponding cmc (D3.5, D5.0, D10.0, D12.0, D15.0, SD2.0, SD4.0, SD6.0, and SD8.0) adding more surfactant (not above cmc) increased the electrostatic repulsive molecular forces when the film thinned down to the level of a black film, stabilizing the latter and thereby increasing the overall lifetime of the films. Of them, for the films of D10.0, D12.0, D15.0, SD6.0, and SD8.0 the entire film turned black before bursting, indicating a strong influence of forces associated with the electric part of the disjoining pressure during the last stage of drainage. However, the time of the onset of the black film did not increase significantly with the increase in concentrations of DTAB and SDS. This shows that the initial gravity-driven drainage flow is not affected strongly by the surfactant concentration below cmc, and the stabilization mechanisms can affect the process only shortly when the films thin to a certain critical thickness.

Note that the results in Tables 1 and 2 show that for the films formed from solutions with surfactant concentrations above cmc (D18.0, D20.0, and SD10.0), lower surface elasticity values were measured than for the corresponding solutions at cmc. This formally stems from the fact that the thinnest initial films were created from micellar solutions as is seen in Figures 9 and 10, and nevertheless, their characteristic drainage times $T$ were rather close to those of the corresponding films at the below-cmc concentrations. Then, according to eq 14, the surface elasticity is diminished. It looks like the surfactant gradient along the surface diminishes when films are initially formed from the above-cmc solutions (since due to stretching the surface concentration in a stretched film still can be lower than the one corresponding to an optimal packing).

The theoretical result, eq 29, revealed a linear decrease in the film thickness during drainage near the film top, which is fully confirmed by the experimental data in Figures 9 and 10. It is emphasized that a linear decrease of the film thickness was also observed experimentally for all other cross sections $x$ at the same rate $dh/dt$ as the one predicted in eq 29.

Despite DTAB and SDS being two radically different surfactants, the former being cationic and the latter anionic, almost identical values were observed for the drainage time of their films. However, the initial thicknesses of the films formed with DTAB solutions were much larger than those of the films of SDS solutions. For the thicker DTAB films the increase in weight was compensated by a higher surface elasticity, which made their drainage time similar to that of the SDS films.

Solutions with different concentrations of nonionic surfactants $C_8E_4$ and nonionic copolymer Pluronic P-123 were also used in experiments with drainage of plane films. For $C_8E_4$ solutions below cmc, an increase in the surfactant concentration led to an increased film lifetime. The films of C0.1, C0.5, C1.0, C7.5 (all below cmc of 7.5 mM) and C10.0 (above cmc) (Figures 11a-11e, respectively) turned completely black before bursting, indicating strong stabilization influence of molecular forces. However, unlike for the plane films formed from the ionic surfactant solutions, the onset time of the black film formation $t_b$ significantly increased with the increase in


dx.doi.org/10.1021/la4003127 | Langmuir 2013, 29, 4934−4947

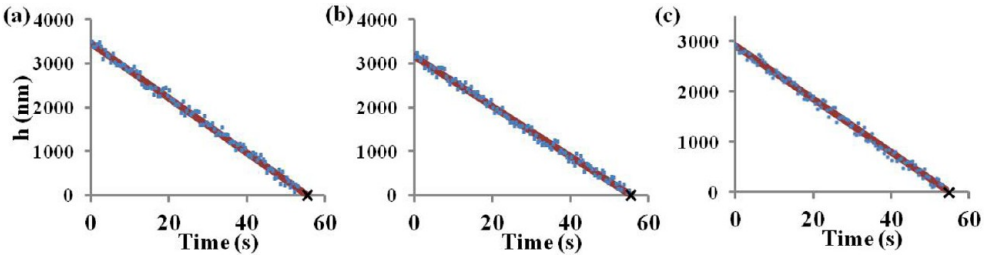


**Figure 12.** Drainage of Pluronic P-123 solution films: (a) P0.052, (b) P0.1, and (c) P0.5. The data correspond to the film top. The experimental results are shown by symbols. The inclined straight lines correspond to the theoretical result, eq 29.

**Table 4. Plane Films of the Nonionic Pluronic P-123 Solutions**[a]

| sol. | $t$ (s) | $t_b$ (s) | $x$ (cm) | $t_{be}$ (s) | $h_i = h_0$ (nm) | $h_{bi}$ (nm) | $T$ (s) | $\varepsilon$ (g/s$^2$) |
|---|---|---|---|---|---|---|---|---|
| P0.052 | 78 | 55 | 4 | 67 | 3461.76 | 3872.93 | 55.31 | 10.93 |
| P0.1 | 72 | 55 | 4 | 65 | 3163.52 | 3574.22 | 55.39 | 9.56 |
| P0.5 | 70 | 54 | 4 | 64 | 2934.55 | 3126.84 | 54.66 | 8.43 |

[a]The film lifetime is denoted $t$; $t_b$ denotes the time at which black film sets in at the top of the wire frame; $t_{be}$ denotes the time at which black film covers the entire wire frame. The $x$ column corresponds to the position in the film (reckoned from the top) to which the leading edge of the black film reached at the moment of bursting. The initial film thickness at the top is denoted $h_i = h_0$, and at the bottom - $h_{bi}$; the drainage time $-T$. The values of the surface elasticity $\varepsilon$ were found from $T$ using eq 14.

concentration. Using the measured values of $T$ and eq 14 to evaluate the surface elasticity $\varepsilon$, it was found that $C_8E_4$ revealed higher values of $\varepsilon$ than ionic surfactants (cf. the data in Table 3 with those of Tables 1 and 2). The drainage of the films formed from $C_8E_4$ solutions was slower than that of the ionic surfactant films. All films of the ionic surfactants studied turned black nearly about the same time depending on the concentration of the surfactant, which determined the total lifetime of the film. For the plane films of the nonionic $C_8E_4$ surfactant, stability of the black films was not affected by the surfactant concentration. The stability of the black films of the nonionic $C_8E_4$ surfactant was low and these black films rapidly burst. The review in ref 44 revealed the results which show that nonionic surfactants, albeit with chains longer than that of $C_8E_4$, are prone to the specific adsorption of hydroxyl ($OH^-$) to the film surfaces. The surfaces thus charged repel each other by electrostatic repulsive forces on the range up to about 100 nm, which adds a stabilizing effect. However, in the present case of a relatively short-chain nonionic $C_8E_4$ surfactant, such stabilization effect on the black-film stage (below 100 nm) was not observed, and the black films rapidly burst. On the other hand, the slower drainage from the nonionic surfactant films compared to the drainage from ionic surfactant films encompassed film thicknesses in the range from 100 to 6000 nm (cf. Figure 11) where any electrostatic repulsive forces associated with specific adsorption of hydroxyl would be negligible. Therefore, the slower drainage from the nonionic surfactant films in the present case can be attributed to a higher surface elasticity, rather than to the electrostatic repulsion. Note also, that even though the formation of the black film was delayed for the nonionic surfactant compared to the ionic ones, the overall lifetime of both types of the films was not very different.

Pluronic P-123 has a very low cmc of 0.052 mM,[34] and solutions of concentrations lower than cmc could not be tested due to the inaccuracy of measuring such low quantities of surfactant. Drainage of plane films was observed for P0.052, P0.1, and P0.5 solutions (Figures 12a − 12c, respectively). For all the concentrations there was no difference between the lifetimes of the films or in their surface elasticities (cf. Table 4).

For both nonionic surfactants ($C_8E_4$ and Pluronic P-123) black films typically appeared after a longer period of time compared to those of the cationic and anionic ionic surfactants DTAB and SDS. Also, the increased values of the drainage time $T$ indicated typically higher values of the surface elasticity of the nonionic surfactants. This is associated with the fact that in the absence of mutual electric repulsion, a higher surface concentration of the nonionic surfactant molecules could be reached compared to the ionic ones, which facilitates higher surface gradients and a stronger Marangoni effect.

**Drainage of Spherical Soap Bubble.** In the experiments single bubbles were formed from Pantene Shampoo solution PS5.0 and four cationic DTAB solutions D5.0, D10.0, D12.0, and D15.0. The experimental data were obtained at the bubble apex at the incidence angle $\theta = 0°$, as mentioned in the section which describes the experimental method. The results on the drainage of spherical bubbles are illustrated in Figure 13 (for the Pantene Shampoo solution PS5.0) and Figure 14 (for the DTAB solutions D5.0, D10.0, D12.0, and D15.0). The latter figure shows that spherical bubbles lasted longer than the

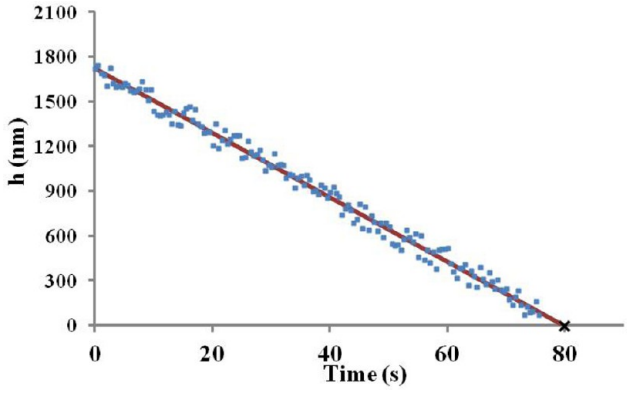


**Figure 13.** Drainage at the top of a spherical bubble of Pantene Shampoo solution PS5.0. The data correspond to the film top (at $\theta = 0°$). The experimental results are shown by symbols. The inclined straight line corresponds to the theoretical result, eq 51.


dx.doi.org/10.1021/la4003127 | Langmuir 2013, 29, 4934−4947

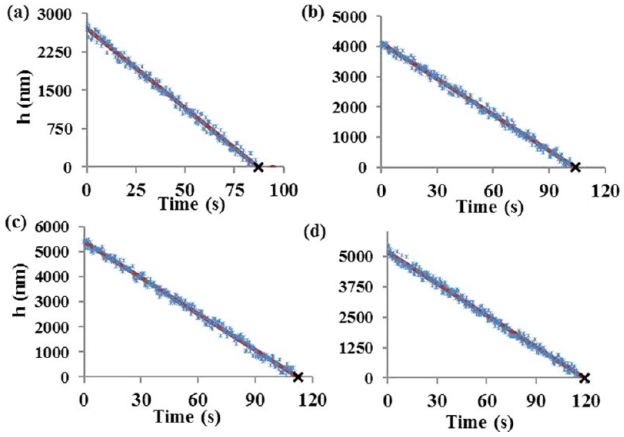


**Figure 14.** Drainage at the top of spherical bubbles of DTAB solutions: (a) D5.0, (b) D10.0, (c) D12.0, and (d) D15.0. The data correspond to the film top (at $\theta = 0°$). The experimental results are shown by symbols. The inclined straight lines correspond to the theoretical result, eq 51.

corresponding plane films. Figures 14a, 14b, 14c, and 14d for spherical bubbles should be compared with the corresponding Figures 9b, 9c, 9d, and 9e for plane films of DTAB, respectively.

The experimental observation that the lifetime of spherical bubbles is about two times longer than the lifetime of the corresponding plane films is in agreement with the predictions of eqs 29 and 51. The results in Figures 13 and 14 allow measuring the drainage time $2T$, which can be used to elucidate the surface elasticity $\varepsilon$ from eq 14. The data for the sperical bubbles are summarized in Table 5, including the values of the

**Table 5. Spherical Bubbles of Pantene Shampoo Solution and DTAB Solutions[a]**

| sol. | $t$ (s) | $t_b$ (s) | $h_i = h_0$ (nm) | $2T$ (s) | $T$ (s) | $\varepsilon$ (g/s$^2$) |
|---|---|---|---|---|---|---|
| PS5.0 | 85 | 78 | 1722.87 | 79.73 | 39.87 | 2.77 |
| D5.0 | 95 | 86 | 2690.31 | 87.15 | 43.58 | 5.89 |
| D10.0 | 118 | 102 | 4121.66 | 103.97 | 51.99 | 13.35 |
| D12.0 | 132 | 110 | 5384.94 | 112.46 | 56.23 | 21.56 |
| D15.0 | 136 | 117 | 5207.73 | 119.31 | 59.66 | 21.75 |

[a]The bubble lifetime is denoted $t$; $t_b$ denotes the time at which black film sets in at the bubble apex. The initial film thickness at the top is denoted $h_i = h_0$, and the drainage time $-2T$. The values of the surface elasticity $\varepsilon$ were found from $T$ using eq 14.

bubble surface elasticity $\varepsilon$. These values of $\varepsilon$ are in good agreement with those found from drainage of plane films of the corresponding surfactant films (cf. Tables 5 and 1).

It took a longer time for spherical bubbles to thin down to a level of a black film that for the corresponding plane films. However, after being formed, black films on spherical bubbles were destabilized faster than the black films on the corresponding plane films. For spherical bubbles, a small black spot appears at the top of the bubble, as the thickness approaches that of the black film and the bubble bursts soon after that.

**Comparison with Data from Literature.** Tables 6 and 7 contain the results of the present work for the surface elasticity $\varepsilon$ of the two ionic surfactants in comparison with the data available in the literature[21,31,45,46] measured by the other methods. In particular, the values of ref 31 were of the same order but higher than the present results (cf. Table 6). The

**Table 6. Comparison of Surface Elasticity $\varepsilon$ Measured for Different Concentrations of Cationic DTAB Solutions with Data in the Literature**

| DTAB solution concns | 3.5 mM | 5 mM | 10 mM | 12 mM | 15 mM | 18 mM | 20 mM |
|---|---|---|---|---|---|---|---|
| present work | 2.49 | 5.78 | 12.87 | 20.74 | 20.27 | 10.6 | 6.86 |
| ref 31 (fitted values $\varepsilon_f$) | 32 | 38 | 60 | - | 40 | - | 38 |

**Table 7. Comparison of Surface Elasticity $\varepsilon$ Measured for Different Concentrations of the Anionic SDS Solutions with Data in the Literature**

| SDS solution concns | 1 mM | 2 mM | 4 mM | 6 mM | 8 mM | 10 mM |
|---|---|---|---|---|---|---|
| present work | - | 0.79 | 1.16 | 2.88 | 4.26 | 2.32 |
| ref 46(the thickest film) | - | - | 27 ± 1 | - | - | - |
| ref 21 | 2.99 | - | - | - | - | - |

surface elasticity values measured for anionic surfactant SDS (cf. Table 7) were in reasonable agreement with those of refs 21 and 45 measured by the microinterferometry method in the Scheludko cell and using the longitudinal surface waves and lower than the one in ref 46 measured using the Wilhelmy plate technique. We found that the surface elasticity values are increasing till the solution cmc contrary to the decreasing trend measured with longitudinal wave viscometer.[47] Surface wave devices operating at lower frequencies consider surface convection to be negligble and surfactant adsorption − desorption and diffusion processes to be predominant, whereas for a soap film in the drainage process, surface convection is more important than the rest.[7] Surfactant solutions above cmc have miscelles formed which contribute to the mass exchange between the surface layer and the bulk phase,[48] resulting in a decrease in surface elasticity, as the present results show. The measured surface elasticity values at cmc of the ionic solutions are significantly lower than those for nonionic surfactants.[24] The increase in surfactant surface diffusion due to repulsion of identical charges and weakening of the Marangoni effect[21] causes faster drainage of the ionic surfactant films.

The values of the surface elasticity $\varepsilon$ measured in the present work for the nonionic surfactant $C_8E_4$ solutions are in reasonable agreement with those of refs 21 and 24 measured for the lower concentrations (cf. Table 8). The values measured

**Table 8. Comparison of Surface Elasticity $\varepsilon$ Measured for Different Concentrations of the Nonionic $C_8E_4$ Solutions with Data in the Literature**

| $C_8E_4$ solution concns | 0.1 mM | 0.5 mM | 1.0 mM | 7.5 mM | 10 mM |
|---|---|---|---|---|---|
| present work | 19.89 | 34 | 54 | 88.27 | 99.59 |
| refs 21 and 24 | 21.1 | - | 211 | - | 1060 |

here are of the same order as those measured for another nonionic surfactant $C_{12}G_2$ in refs 49 and 50. The values of the surface elasticity $\varepsilon$ measured for Pluronic P-123 are quite comparable with the values measured in ref 49 for the other Pluronics, namely Pluronic F-68 and Pluronic F-127 (Table 9).

The surface elasticity of a longer nonionic surfactant $C_{12}E_6$ measured in ref 51 in the concentration range $0.1 \leq c/\text{cmc} \leq 1$ (with $c$ being surfactant concentration) belong to the range 30 to 40 g/s$^2$, whereas our data in Tables 3 and 8 for a shorter


dx.doi.org/10.1021/la4003127 | Langmuir 2013, 29, 4934−4947

**Table 9. Comparison of Surface Elasticity $\varepsilon$ Measured for Different Concentrations of the Nonionic Pluronic P-123 Solutions with Data in the Literature**

| solution concns | 0.052 mM | 0.1 mM | 0.5 mM | 0.6 mM | 1.0 mM |
|---|---|---|---|---|---|
| Pluronic P-123 (present work) | 10.93 | 9.56 | 8.43 | - | - |
| Pluronic F-68 (ref 40) | - | - | - | 21 ± 1.6 | - |
| Pluronic F-127 (ref 40) | - | - | - | - | 22.1 ± 1.6 |

nonionic surfactant $C_8E_4$ reveal $19.89 \leq \varepsilon \leq 54$ g/s$^2$ in the range $0.013 \leq c/\mathrm{cmc} \leq 0.13$ and $\varepsilon = 88.27$ g/s$^2$ at $c/\mathrm{cmc} = 1$. This shows that our data for $C_8E_4$ are in good agreement with the data for $C_{12}E_6$ at relatively low surfactant concentration and probably overestimates $\varepsilon$ at cmc, since $\varepsilon$ is expected to increase with chain length.[51]

## CONCLUSIONS

We developed a method of measuring the surface elasticity of surfactant films using gravity-driven drainage from plane vertical films suspended on a wire frame or from a spherical bubble located on the free surface of a liquid pool. The method is based on the theory proposed in this work. The physical pattern of the drainage due to gravity and the effect of the surface elasticity on it is the following. The upper part of the film is stretched by the weight of the film suspended on it. As a result, surfactant concentration is diminished at the surface of the upper part of the film, and surface tension there is higher than in the lower section of the film which is stretched less. The higher surface tension in the upper part of the film results in the Marangoni stress directed upward which opposes gravity-driven drainage. Therefore, the duration of the drainage process is determined by the competition of gravity and the Marangoni stress and could be employed to measure the surface elasticity $\varepsilon$. Moreover, the usage of relatively thick films allows the exclusion of a potentially stabilizing electrostatic forces for practically the entire duration of drainage from the ionic and nonionic surfactant films (the latter can be prone to specific adsorption of hydroxyl at the film surface).

The surface elasticity values measured in plane films of cationic surfactant DTAB and anionic surfactant SDS increased with an increase in surfactant concentration until cmc was reached and were found to be maximal at cmc. Below cmc, an increase in the surfactant concentration in the bulk was accompanied by an increase in the surfactant concentration gradient at the film surface, thereby increasing the surface elasticty. Above cmc, the results suggest that the surfactant gradient along the surface diminishes when films are initially formed (since due to stretching, the surface concentration in a stretched film still can be lower than the one corresponding to an optimal packing), and the surface elasticity is lower than the one at cmc.

Similar trends were observed with plane films of nonionic surfactants $C_8E_4$ and Pluronic P-123. Due to its small cmc value, the experiments with Pluronic P-123 could not be done for concentrations below cmc. However, similarly to the ionic surfactant, the surface elasticity values for Pluronic P-123 decreased with an increase in its concentration above cmc. Higher surface elasticity values for nonionic surfactant $C_8E_4$ were measured as compared to the values for the ionic surfactants DTAB and SDS, and the values increased as the surfactant concentration increased.

The spherical bubbles formed with DTAB solutions lasted almost twice the time of the corresponding plane films because the effect of gravity is less pronounced in the drainage from spherical bubbles (note, that the flow is horizontal near the apex and inclined over the rest of the generatrix). The surface elasticity values of DTAB solutions measured for plane films and spherical bubbles were close to each other, indicating that surface elasticity plays the principal role in drainage of thin films as well as the self-consistency of our two methods of measurements based on plane or spherical films.

## AUTHOR INFORMATION

### Corresponding Author

*Phone: +1(312) 996-3472. Fax: +1(312) 413-0447. E-mail: ayarin@uic.edu.

### Notes

The authors declare no competing financial interest.

## ACKNOWLEDGMENTS

This work was partially supported by The US Gypsum Corporation (USG).

## REFERENCES

(1) Scheludko, A. Thin liquid films. *Adv. Colloid Interface Sci.* **1967**, *4*, 391−464.
(2) Derjaguin, B. V.; Churaev, V. N.; Muller, V. M. *Surface Forces*; Plenum Press: New York, 1987.
(3) Derjaguin, B. V. *Theory of Stability of Colloids and Thin Films*; Consultants Bureau/Plenum Publishing Co.: New York, 1989.
(4) Levich, V. G. *Physicochemical Hydrodynamics*; Prentice Hall: Englewood Cliffs, 1962.
(5) Israelachvili, J. *Interfacial and Surface Forces*; Academic Press: London, 1992.
(6) Edwards, D. A.; Brenner, H.; Wasan, D. T. *Interfacial Transport Phenomena*; Butterworth-Heinemann: Boston, 1991.
(7) Langevin, D.; Sonin, A. A. Thinning of soap films. *Adv. Colloid Interface Sci.* **1994**, *51*, 1−27.
(8) Valkovska, D. S.; Danov, K. D.; Ivanov, I. B. Stability of draining plane-parallel films containing surfactants. *Adv. Colloid Interface Sci.* **2002**, *96*, 101−129.
(9) Weaire, D.; Hutzler, S. *The Physics of Foams*; Oxford University Press: Oxford, 1999.
(10) Morrison, I. D.; Ross, S. *Colloidal Dispersions: Suspensions, Emulsions and Foams*; Wiley Interscience: New York, 2002.
(11) *Interfacial Rheology*; Miller, R., Liggieri, L., Eds.; Brill: Leiden, 2009.
(12) Exerova, D.; Kruglyakov, P. M. *Foam and Foam Films. Theory, Experiment, Application*; Elsevier: Amsterdam, 1998.
(13) Nguyen, A. V.; Schulze, H. J. *Colloidal Science of Floatation*; Marcel Dekker, Inc.: 2004.
(14) Murray, B. S.; Ettelaie, R. Foam stability: proteins and nanoparticles. *Curr. Opin. Colloid Interface Sci.* **2004**, *9*, 314−320.
(15) Hunter, T. N.; Pugh, R. J.; Franks, G. V.; Jameson, G. J. The role of particles in stabilizing foams and emulsions. *Adv. Colloid Interface Sci.* **2008**, *137*, 57−81.
(16) Dickinson, E. Food emulsions and foams: stabilization by particles. *Curr. Opin. Colloid Interface Sci.* **2010**, *15*, 40−49.
(17) Karakashev, S. I.; Nguyen, A. V.; Manev, E. D.; Phan, C. M. Surface foam film waves studied with high-speed linescan camera. *Colloids Surf., A* **2005**, *262*, 23−32.
(18) Karakashev, S. I.; Nguyen, A. V.; Manev, E. D. A novel technique for improving interferometric determination of emulsion film thickness by digital filtration. *J. Colloid Interface Sci.* **2007**, *306*, 449−453.

(19) Karakashev, S. I.; Manev, E. D.; Tsekov, R.; Nguyen, A. V. Effect of ionic surfactants on drainage and equilibrium thickness of emulsion films. *J. Colloid Interface Sci.* **2008**, *318*, 358−364.
(20) Karakashev, S. I.; Nguyen, A. V. Do liquid films rupture due to the so-called hydrophobic force or migration of dissolved gases? *Langmuir* **2009**, *25*, 3363−3368.
(21) Karakashev, S. I.; Ivanova, D. S. Thin film drainage: ionic vs. non-ionic surfactants. *J. Colloid Interface Sci.* **2010**, *343*, 584−593.
(22) Karakashev, S. I.; Stockelhuber, K. W.; Tsekov, R. Wetting films on chemically patterned surfaces. *J. Colloid Interface Sci.* **2011**, *363*, 663−667.
(23) Karakashev, S. I.; Manev, E. D.; Nguyen, A. V. Effect of double-layer repulsion on foam drainage. *Colloids Surf., A* **2008**, *319*, 34−42.
(24) Karakashev, S. I.; Ivanova, D. S.; Angarska, Z. K.; Manev, E. D.; Tsekov, R.; Radoev, B.; Slavchov, R.; Nguyen, A. V. Comparative validation of the analytical models for the Marangoni effect on foam film drainage. *Colloids Surf., A* **2010**, *365*, 122−136.
(25) Debregeas, G.; de Gennes, P. G.; Brochard-Wyart, F. The life and death of "bare" viscous bubbles. *Science* **1998**, *279*, 1704−1707.
(26) de Gennes, P. G. "Young" soap films. *Langmuir* **2001**, *17*, 2416−2419.
(27) Koehler, S. A.; Hilgenfeldt, S.; Stone, H. A. A generalized view of foam drainage: experiment and theory. *Langmuir* **2000**, *16*, 6327−6341.
(28) Jun, S.; Pelot, D. D.; Yarin, A. L. Foam consolidation and drainage. *Langmuir* **2012**, *28*, 5323−5330.
(29) Kornev, K. G.; Neimark, A. V.; Rozhkov, A. N. Foam in porous media: thermodynamic and hydrodynamic peculiarities. *Adv. Colloid Interface Sci.* **1999**, *82*, 127−187.
(30) Bazilevsky, A. V.; Rozhkov, A. N. Motion of a foam lamella in a circular channel under a relaxing small pressure jump. *Colloids Surf., A* **2012**, *414*, 457−465.
(31) Sonin, A. A.; Bonfillon, A.; Langevin, D. Thinning of soap films: the role of surface viscoelasticity. *Colloid Interface Sci.* **1994**, *162*, 323−330.
(32) Berg, S.; Adelizzi, E. A.; Troian, S. M. Experimental study of entrainment and drainage flows in microscale soap films. *Langmuir* **2005**, *21*, 3867−3876.
(33) Mysels, K. J. Surface tension of solutions of pure sodium dodecyl sulfate. *Langmuir* **1986**, *2*, 423−428.
(34) Alexandridis, P.; Holzwarth, J. F.; Hatton, T. A. Micellization of poly(ethylene oxide) − poly(propylene oxide) − poly(ethylene oxide) triblock copolymers in aqueous solutions: thermodynamics of copolymer association. *Macromolecules* **1994**, *27*, 2414−2425.
(35) Afanasyev, Y. D.; Andrews, G. T.; Deacon, C. G. Measuring soap bubble thickness with color matching. *Am. J. Phys.* **2011**, *79*, 1079−1082.
(36) Mysels, K. J. Dynamic processes in soap films. *J. Gen. Physiol.* **1968**, *52*, 113−124.
(37) Mysels, K. J.; Shinoda, K.; Frankel, S. *Soap Films. Studies of Their Thinning and a Bibliography*; Pergamon Press: London, 1959.
(38) Nierstrasz, V. A.; Frens, G. Marginal regeneration and the Marangoni effect. *J. Colloid Interface Sci.* **1999**, *215*, 28−35.
(39) Nierstrasz, V. A.; Frens, G. Marangoni flow driven instabilities and marginal regeneration. *J. Colloid Interface Sci.* **2001**, *234*, 162−167.
(40) Berg, S.; Adelizzi, E. A.; Troian, S. M. Images of the floating world: patterns in thinning soap films. *Phys. Fluids* **2004**, *16*, S6.
(41) Taylor, G. I. The dynamics of thin sheets of fluid. III. Disintegration of fluid sheets. *Proc. R. Soc. London* **1959**, *A253*, 313−321.
(42) Culick, F. E. C. Comments on a rupture soap film. *J. Appl. Phys.* **1960**, *31*, 1128−1129.
(43) Lurie, A. I. *Theory of Elasticity*; Springer: Berlin, 2005.
(44) Stubenrauch, C.; von Klitzing, R. Disjoining pressure in thin liquid foam and emulsion films- new concepts and perspectives. *J. Phys.: Condens. Matter* **2003**, *15*, R1197−R1232.
(45) Noskov, B. A.; Aleksandrov, D. A.; Gumennik, E. V.; Krotov, V. V.; Miller, R. The dynamic surface elasticity of sodium dodecyl sulfate solutions in the frequency range 0.8−5 Hz. *Colloid J.* **1998**, *60*, 204−210.
(46) Prins, A.; Arcuri, C.; Van Den Tempel, M. Elasticity of thin liquid films. *J. Colloid Interface Sci.* **1967**, *24*, 84−90.
(47) Rao, A. A.; Wasan, D. T.; Manev, E. D. Foam stability − effect of surfactant composition on the drainage of microscopic aqueous films. *Chem. Eng. Commun.* **1982**, *15*, 63−81.
(48) Noskov, B. A.; Alexandrov, D. A.; Miller, R. Dynamic surface elasticity of miscellar and nonmiscellar solutions of dodecyldimethyl phosphine oxide. Longitudinal wave study. *J. Colloid Interface Sci.* **1999**, *219*, 250−259.
(49) Georgieva, D.; Cagna, A.; Langevin, D. Link between surface elasticity and foam stability. *Soft Matter* **2009**, *5*, 2063−2071.
(50) Santini, E.; Ravera, F.; Ferrari, M.; Stubenrauch, C.; Makievski, A.; Kragel, J. A surface rheological study of non-ionic surfactants at the water-air interface and the stability of the corresponding thin foam films. *Colloids Surf., A* **2007**, *298*, 12−21.
(51) Stubenrauch, C.; Shrestha, L. K.; Varade, D.; Johansson, I.; Olanya, G.; Aramaki, K.; Claesson, P. Aqueous foam stabilized by n-dodecyl-$\beta$-D-maltoside, hexaethyleneglycol monododecyl ether, and their 1:1 mixture. *Soft Matter* **2009**, *5*, 3070−3080.